Digital Applications in Archaeology and Cultural Heritage 5 (2017) 10–20

Contents lists available at ScienceDirect

Digital Applications in Archaeology and Cultural Heritage

journal homepage: www.elsevier.com/locate/daach

Combining geometrical and radiometrical features in the evaluation of rock art paintings

Jose Alberto Torres-Martínez[a], Luis Javier Sánchez-Aparicio[a,*], David Hernández-López[b], Diego González-Aguilera[a]

[a] Department of Land and Cartographic Engineering. University of Salamanca, High Polytechnic School of Avila, Hornos Caleros, 50, 05003 Avila, Spain
[b] Regional Development Institute-IDR, University of Castilla-La Mancha, 02071 Albacete, Spain

ARTICLE INFO

Keywords:
Rock art
Terrestrial Laser Scanner
Close-range Photogrammetry
Multispectral camera
Radiometric classification
Geometrical features

ABSTRACT

Rock art painting is one of the most ancient manifestation of Cultural Heritage. Its fragility demands the use of non-destructive methods for the evaluation of engraved or painted signs contained in caves or shelters. However, most of existing approaches involve the exploitation of radiometric information coming from digital images captured by RGB cameras, showing several drawbacks such as: (i) lack of scale; (ii) lack of flexibility and (iii) high user interaction, among others. In order to provide added value to these approaches, this paper describes a methodology able to combine radiometrical and geometrical features captured by different geomatic sensors (multispectral cameras and terrestrial laser scanner), allowing not only the extraction of the painted signs presented, but also evaluating different aspects of great importance in the understanding of rock art (e.g. the presence of topographic accidents that could influence on the painted signs traces or its visibility under different illumination conditions).

1. Introduction

Nowadays, Cultural Heritage is considered a keystone of the modern society (Herbert, 1995), becoming its preservation a hot topic for the Scientific Community (Del Pozo-Aguilera et al., 2016; Rodríguez-Gonzálvez et al., 2015). From the digitalization of architectural monuments (Sánchez-Aparicio et al., 2014) and prehistoric caves (Azema et al., 2013; Fritz et al., 2016; Puchol et al., 2013, Rodríguez-Gonzálvez et al., 2012), to the aerial surveying of archeological settlements (Fernández-Hernandez et al., 2015, Gomez-Lahoz and González-Aguilera, 2009), geomatics sensors has been widely tested as a tool for Cultural heritage conservation, either alone or in combination (Aguilera et al., 2006; Torres-Martínez et al., 2016).

Inside the wide diversity of monuments, sculptures, paintings, etc. that make up our Cultural Legacy, the rock art paintings or engravings are one of the most ancient manifestations of the humanity. These works, which date from at least 40,000 years, were made on rock surfaces (Bourdier et al., 2015; Robert et al., 2016), suffering a constant degradation by agents such as the water or the atmosphere. The use of non-contact techniques allow us to evaluate not only the paintings or engravings presented (Burens et al., 2011; Defrasne, 2014; Pinçon et al., 2010), but also aspects such as the presence of non-accesible areas or the influence of the topographic accidents in the painted or engraved traces (Lejeune, 1985; López-Montalvo and Sanz, 2005; Robert, 2016, Sauvet et al., 1998). These considerations place the geomatic sensors, such as the Terrestrial Laser Scanner (TLS) or the digital cameras, as the most suitable solutions for the recording of these art manifestations (Seidl et al., 2015; Zeppelzauer et al., 2015).

Regarding TLS, its characteristics can offer a wide range of advantages such as the non-contact nature, the fast data acquisition or the non-light conditions required to capture the data. As a result, large and complex sites can be recorded in 3D in a short period of time. Additional to these geometrical measurements, TLS systems can also record intensity values related with the wavelength used. On the other hand, RGB and multispectrals sensors allow the capture of a variety of different wavelengths and also enable for the 3D reconstruction of complex sites using approaches such as Structure from Motion (SfM), a technique that has proven to be an appropriate solution in archaeologial works (Cefalu et al., 2013; Lerma et al., 2013) since it combines the advantages of the computer vision (automation and flexibility) and photogrammetry (accuracy and reliability) and whose accuracy and resolution can compete with those obtained by the TLS systems (Rodríguez-Gonzálvez et al., 2014).

However, common strategies for the evaluation of the paintings

* Corresponding author.
E-mail addresses: josealberto@usal.es (J.A. Torres-Martínez), luisj@usal.es (L.J. Sánchez-Aparicio), david.hernandez@uclm.es (D. Hernández-López), daguilera@usal.es (D. González-Aguilera).

http://dx.doi.org/10.1016/j.daach.2017.04.001
Received 5 December 2016; Received in revised form 25 March 2017; Accepted 18 April 2017
Available online 20 April 2017

presented in the rock art are limited to the use of decorrelation strategies (e.g. Decorrelation Strech-DS or principal component analysis-PCA) of images captured by RGB sensors (Cerrillo-Cuenca and Sepúlveda, 2015; Domingo et al., 2015) that only use the single radiometric response captured by the sensors. Although the use of orthoimages and unsupervised pixel-based classifications can provide a suitable solution (Rogerio-Candelera, 2015), the geometrical and radiometrical features of both products are not exploited or combined together to support the final solution. For instance, voids or topographic accidents can generate shadows that distort the multispectral classification results, requiring the use of additional strategies able to filter these problems.

A complete study of the paintings presented on a rock art shelter demands not only the evaluation of the painted or engraved signs, but also to record these signs through accurate 3D virtual models able to reproduce hypotetic situations such as: to simulate different illumination conditions or to analyse spatial geometrical relations (e.g. the relation between the depth an the areas painted) (Domingo et al., 2013).

According to remarked above, this paper presents a methodology for combining geometrical and radiometrical features in the evaluation of rock art paintings presented in a shelter using two different scales: (i) *a local scale*, looking over all those properties needed for a complete understanding of the traces presented for each motif; and (ii) *a global scale,* to evaluate the whole shelter and its spatial relationship with the existing motifs. To validate this approach, a phase-shift laser scanner (Faro Focus 120), a full frame reflex camera (Canon 5D) and a multispectral camera (Mini MCA 6) were applied in the evaluation of the painted sings presented in the Minateda Great shelter (Albacete, Spain), one of the most important Levantine Rock art shelters (Breuil, 1920; Mas et al., 2013).

This paper has been organized in the following way: after this introduction, Section 2 presents the sensors and methods used during the evaluation of the rock-shelter; Section 3 shows the results of the proposed methodology and finally in Section 4 depicts the main conclusions.

2. Materials and methods

In this section the three geomatics sensors used in this work together with the approach developed are described.

2.1. Materials

2.1.1. Terrestrial laser scanner sensor: Faro Focus 120

Considering the complexity of the shelter as well as its difficult accessibility the TLS Faro Focus 120 (Table 1) was used.

Due to the size of the shelter (19.59 × 3.65 m) evaluated, several TLS stations were considered, each one placed on an arbitrary local coordinate system. The registration of these stations into a common local coordinate system was performed using a coarse to fine strategy defined in Sánchez-Aparicio et al. (2014). As a result of this registration an accurate 3D representation of the shelter, in the near infrared band, was obtained.

Table 1
Faro Focus 120 technical specifications.

Physical principle	Phase shift
Field of view (degrees)	360 H x 320 V
Measurement range (m)	0.6 − 120
Accuracy nominal value at 25 m (mm)	2
Beam divergence (mrad)	0.19
Capture rate (points/sec)	122,000 / 976,000
Spatial resolution at 10 m (mm)	6
Wavelength (nm)	905 / near infrared
Radiometric resolution (bits)	11- bits

Table 2
Canon 5D Mk II technical specifications.

Sensor type	CMOS
Sensor size (mm)	36 × 24
Image size (pixels)	5616 × 3744
Geometric resolution (Mp)	21.1
Pixel size (μm)	6.4
Focal length (mm)	20
Radiometric resolution	14 bits
Channels	Red, Green, Blue

Table 3
Mini MCA-6 technical specifications.

Sensor type	CMOS
Sensor size (mm)	6.7 × 5.3
Image size (pixels)	1280 × 1024
Geometric resolution (Mp)	1.3
Pixel size (μm)	5.2
Focal length (mm)	9.6
Radiometric resolution	10 bits

2.1.2. Digital camera sensors: Canon 5D and Mini MCA-6

Two passive sensors were used and evaluated: a full frame RGB reflex digital camera (Canon 5D Mk II) and a multispectral digital camera (Mini MCA-6).

Equipped with a Canon EF 20 mm wide-angle lens, Canon 5D Mk II is a high resolution full frame reflex camera (Table 2) capable of capturing visible information in the following wavelengths: (i) Red-650 nm; (ii) Green-532 nm; and (iii) Blue-473 nm.

Regarding the multispectral sensor, a lightweight Multiple Camera Array (Mini MCA-6) was used. This sensor includes a total of 6 individual CMOS sensors with filters for the visible and near infrared spectrum (NIR) (Table 3), allowing the acquisition of a wide range of wavelengths: (i) Green-530 nm; (ii) Red1–672 nm; (iii) Red2–700 nm; (iv) NIR1–742 nm; (v) NIR2–778 nm; and (vi) NIR3–801 nm.

2.2. Methodology

In the present study case a standard SfM procedure, implemented in the photogrammetric software GRAPHOS (González-Aguilera et al., 2016), was applied for the photogrammetric 3D model generation, comprising the following stages: (i) automatic extraction and key-point matching; (ii) hierarchical orientation of images; and (iii) dense point cloud generation.

As a result, a dense and accurate point cloud can be obtained from the multiple images acquired where each pixel in the image renders a 3D point of the object.

Given the high density of points provided by both approaches (laser scanning and SfM) the orthogonal projection of these points provides the generation of digital images with metric values (orthoimages), corrected from geometrical distortions and perspective effects. Based on these orthoimages pixel-based classification strategies were applied through the use of statistical methods (e.g. Maximum Likelihood or Fuzzy k-means algorithms), which deal with multispectral bands to extract informational classes from the orthoimages generated, allowing more flexibility and less user interaction than decorrelation methods.

Although pixel-based approaches provide more flexibility and less user interaction than decorrelation methods, they can be influenced by the presence of geometrical accidents such as voids, elevation or cracks, causing the creation of local shadows and thus disturbing the final classification results. Geometrical accidents can be related with local

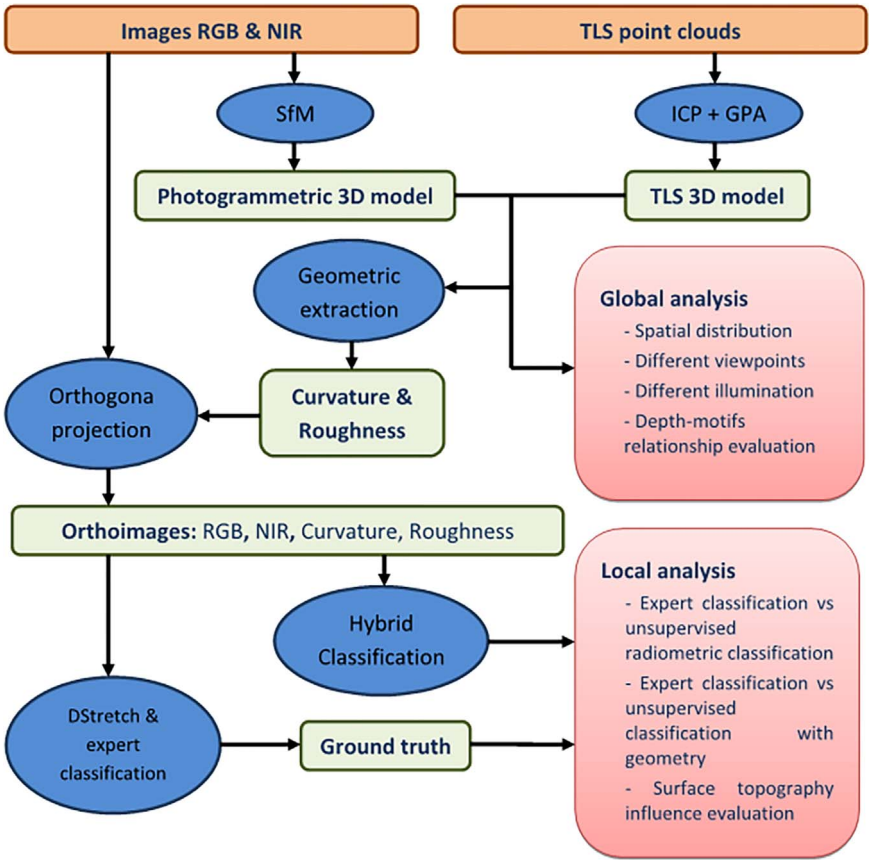

Fig. 1. Workflow for the proposed methodology.

Fig. 2. Case study area: Great shelter of Minateda (Spain).

changes in the curvature of the rock surface or even with roughness changes. According with these assumptions and considering the flexibility provided by the pixel-based methods, the Gaussian curvature (Magid et al., 2007) as well as the roughness of the point cloud were considered to support the pixel-based classification. Regarding the roughness, several local PCA analysis were carried out with the aim of extracting the direction of minimum dispersion (first Eigen-vector) which corresponds with the normal of the points considered (Rodríguez-Martín et al., 2016). Later the roughness is estimated evaluating the distance between the plane, defined with the centroid of the point cloud and the first Eigen vector, and each point considered.

It is worth mentioning, that the classification of pixels according with their radiometrical and geometrical response is not the only requirement to evaluate the rock art paintings. Geometrical components, such as the distribution of motifs along the shelter, the spatial relation between motifs, the influence of the topographic accidents in the traces of motifs, or the relation between the shelter depth and the motifs distribution are aspects that have been analyzed. More precisely, the evaluation of the digital depth model and its contour lines associated were used to analyse the motifs traces and its relationship with the main contour lines. In addition, the digital depth model and its 3D model were used to analyse the spatial distribution of motifs along the shelter and also to simulate virtual viewpoints of the shelter and the motifs with different lightning conditions.

A graphical summarize of the whole process is shown in Fig. 1.

3. Experimental results

3.1. Minateda rock-shelter

Located in the Archeological Park of Tolmo de Minateda near the city of Hellín, within the province of Albacete (Spain), Minateda Great Shelter is placed on a strategic area between the West and East part of the Iberian Peninsula (Montés, 2010) (Fig. 2). This localization gives the shelter a blending of different artistic tendencies. Showing more than 400 motifs painted on a Miocenic biocalcerinite formation, with a

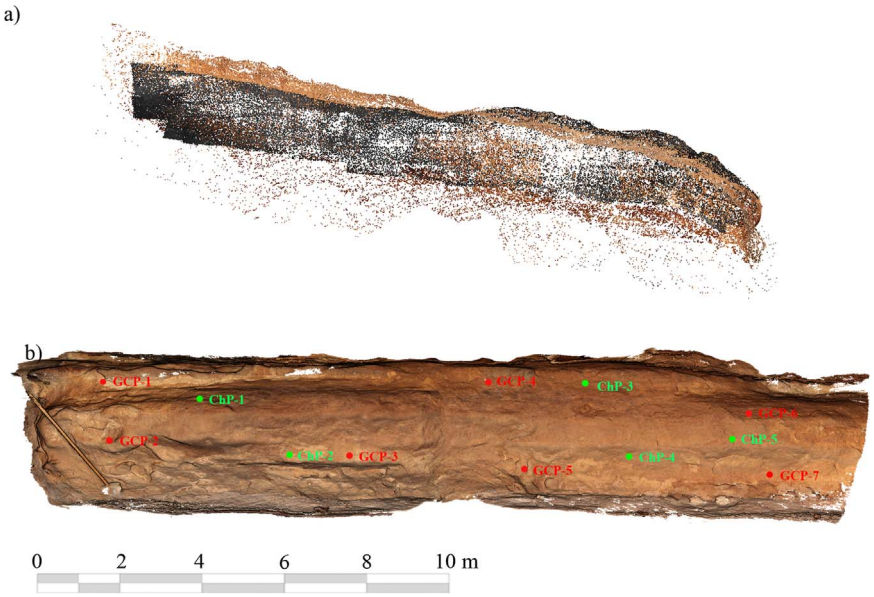

Fig. 3. Results obtained during the SfM approach: (a) Sparse point cloud obtained during the orientation; and (b) 3D dense point cloud and distribution of the control points (in red colour) and check points (in green colour). (For interpretation of the references to color in this figure legend, the reader is referred to the web version of this article.)

Table 4
RMSE and errors obtained during the photogrammetric reconstruction.

Point name	*X* error (mm)	*Y* error (mm)	*Z* error (mm)
ChP−1	−1.43	−0.19	1.53
ChP−2	5.99	−2.15	0.29
ChP−3	−4.43	−1.19	−0.96
ChP−4	0.51	−0.00	−0.63
ChP−5	0.18	−0.19	1.53
RMSE	3.40	1.96	1.09

total length of 20 m and 8 m of height. Inside this space, several narrative natural scenes are presented, as well as motifs of hunting and battles (Breuil, 1920), establishing the Minateda Great Shelter as one of the most important Spanish Levantive rock-art shelter (Mas et al., 2013).

3.2. Multispectral point clouds

According with the sensors used, two point clouds were generated: (a) Laser scanning point cloud and (b) Multispectral photogrammetric point cloud.

Regarding the laser scanning, eight laser stations were required and aligned using a coarse-to fine, comprising the following stages: (i) pairwise registration through the Iterative Closest Point (ICP) algorithm (Besl and McKay, 1992) and (ii) a global registration by means of the Generalized Procrustes Analysis (GPA) (Toldo et al., 2010), using the ICP registration as initial approximation. As a result, a complete 3D point cloud of the rock-shelter in the near infrared (905 nm) with a total of 82,244,854 points and a registration error of 0.003 ± 0.001 m, was obtained.

Regarding the photogrammetric point clouds, one of the main milestones of the photogrammetric technique is its flexibility to cope with different spectral bands captured with different sensors. However, deal with different sensors requires taking into account the following considerations:

- Type of sensor. Meanwhile the Canon 5D presents a unique Bayer sensor, the Mini MCA-6 camera shows six different CMOS sensors with specific filters and lenses. Each MCA camera station is composed by 6 images with different intrinsic (principal distance, principal point and lens distortion) and extrinsic (location and orientation) parameters. According with Kraus (2007), the baseline between stations is a critical factor in the final accuracy of the

Fig. 4. Graphical comparison between point clouds: (a) coming from TLS; and (b) coming from digital camera.

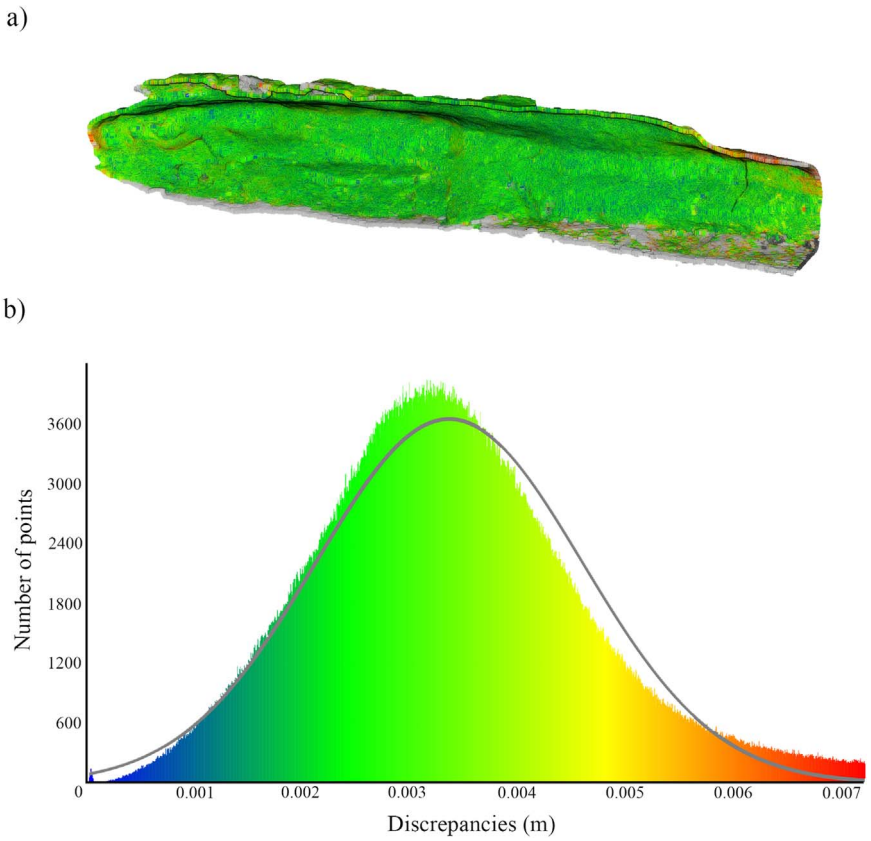

Fig. 5. Geometrical discrepancies between the laser and photogrammetric point cloud: (a) Comparison between 3D models (laser vs. photogrammetry); and (b) histogram of errors distribution.

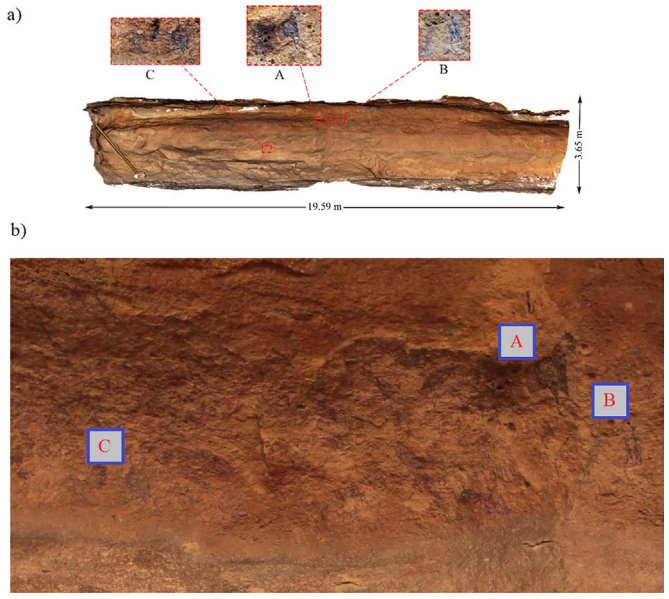

Fig. 6. Test areas (A, B, C) used during the evaluation of bands. (a) Distribution within the shelter; (b) Detail of the test area.

photogrammetric point cloud. Therefore, introduce in the photogrammetric adjustment the different channels of the multispectral camera would provide an unsuitable base to ratio value. With the aim of optimizing this problem, only the fifth channel (lower-center cone) of the multispectral camera was considered for the photogrammetric reconstruction, registering the rest of the channels against this one. To this end, the following workflow was applied: (i) Geometrical calibration of the images; (ii) Key-point extraction and matching and (iii) Affine transformation. As a result, several multiband images were obtained, corrected from geometrical distortions and registered in relation with the fifth channel, throwing a mean registration error of 0.79 ± 0.52 pixels.

- Photogrammetric network design. Guarantee quality in the 3D photogrammetric models requires of planning a good photogrammetric stations distribution (i.e. network). In particular, two different groups of images were considered: (i) parallel images and (ii) convergent images. 215 images were acquired with the Canon 5D, whereas 90 images were taken with the Mini MCA-6. Regarding the MCA-6 sensor, the images acquired were focused on the painted area of the shelter.
- Multimodal matching. Since the approach developed requires the use of algorithms able to extract and matching keypoints at different spectrums (i.e. images coming from different wavelengths), a modification of the usual features extraction method (Lowe, 1999), was applied. More precisely, the keypoint detector and descriptor MSD (Tombari and Di Stefano, 2014) and SURF (Bay et al., 2008) were applied, respectively, using a robust matching strategy implemented in the software GRAPHOS.

Finally, multispectral and RGB images captured by MCA-6 and Canon 5D, respectively, were used as input in the SfM workflow using GRAPHOS software. Regarding MCA images, null values were considered for the distortion parameters and the principal point (these values remain fixed during the SfM approach).

During the first phase (orientation) a sparse point cloud composed by 101,122 keypoints was obtained. Concerning the scaling of the point cloud, 7 control points and 5 check points were used from the laser scanning point cloud using artificial targets (Fig. 3) (Table 4).

Finally, a dense matching was carried out by means of the MicMac algorithm (Pierrot-Deseilligny et al., 2015) obtaining as a result a dense

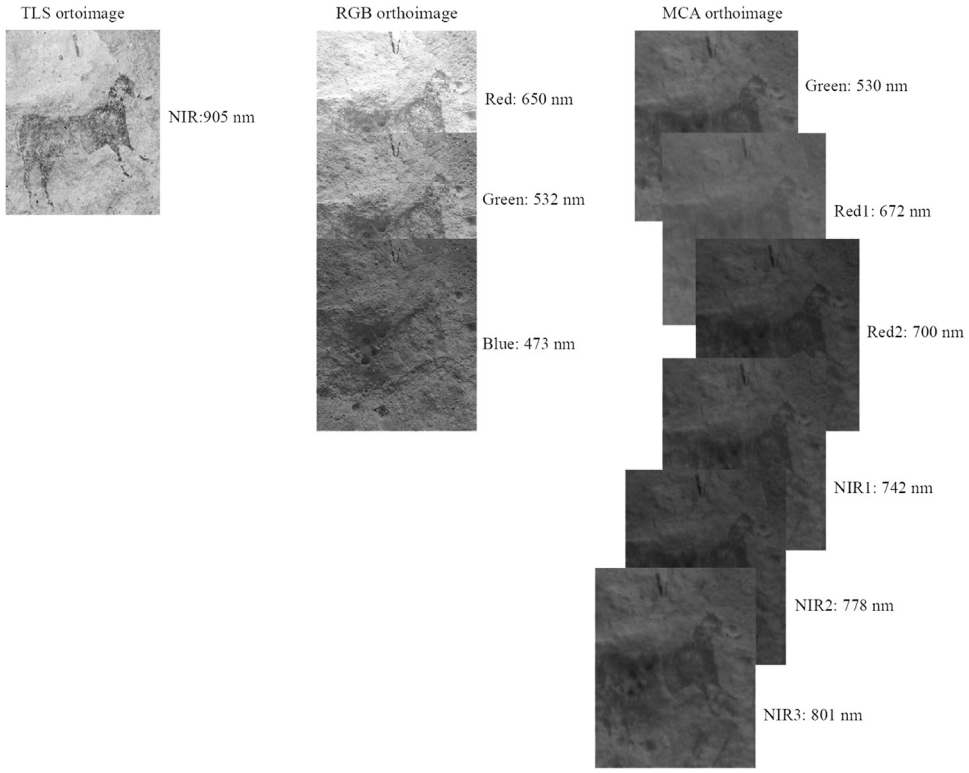

Fig. 7. Graphical representation of the different multispectral orthoimages generated.

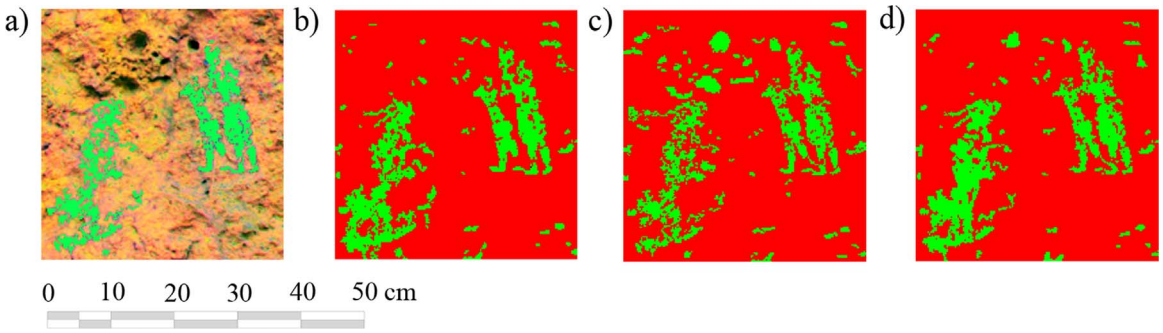

Fig. 8. Results obtained during the first phase for the test area B: (a) Decorrelation; (b) LS band; (c) 5D band and (d) MCA-6 band. Red pixels correspond with the background informational class and green pixels with the motif informational class. (For interpretation of the references to color in this figure legend, the reader is referred to the web version of this article.)

Table 5
Percentage of pixels belonging to the motif informational class.

Method	Sensor	A (%)	B (%)	C (%)
Decorrelation (Ground Truth)	Canon 5D	15.60	10.64	19.28
Unsupervised classification	Laser Scanner	17.89	15.59	20.40
	Canon 5D	17.88	15.37	19.37
	Mini MCA − 6	18.07	15.77	18.98

and photorealistic point cloud of the rock-shelter, whose quality (0.003 ± 0.001 m) and density (74,457,717 points) is similar to the one provided by the TLS point cloud (82,244,854 points) (Fig. 4) (Fig. 5).

3.3. Unsupervised pixel-based classification for the extraction of motifs

Due to the large number of bands as well as the complexity and extension of the rock-shelter, three test areas (A, B, C) were used for the evaluation of the best band combination. These areas were considered according to the geometrical accidents presented on it. For the test area A is possible to observe the presence of voids inside and near the motifs; for the test area B the voids are near the motif; and for the test area C no voids are near or inside the motif (Fig. 6).

Obtained the different radiometric bands (a total of 9 images with a 2 mm of GSD), a pixel-based classification was performed using the multispectral orthoimages as input data (Fig. 7). Since each sensor encloses its own resolution, the multispectral orthoimages were homogenized to a 2 mm resolution. The non-supervised Fuzzy-k-means algorithm was used following the next combination of bands: (i) 1st band from laser scanner (LS band); (ii) 2nd 3rd and 4th bands from Canon 5D (5D band); and (iii) 5th, 6th, 7th, 8th, 9th and 10th bands from Mini MCA-6 (MCA-6 band).

During the first phase of the radiometric analysis, which considers only the radiometric response captured by the different sensors, two informational classes were evaluated: Motif and Background. Complementary to this, the results obtained using decorrelation of RGB channels by means of the Decorrelation Stretch algorithm (Le Quellec et al., 2015) supported by a manual classification of an expert

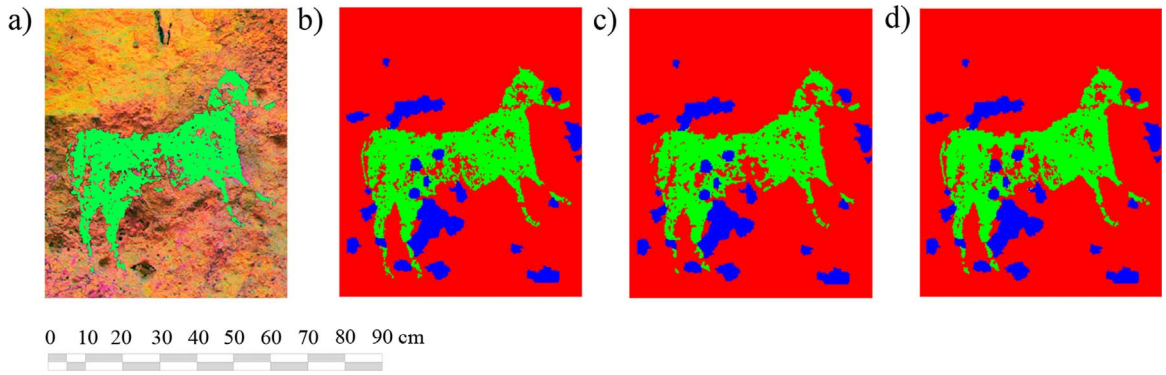

Fig. 9. Multispectral classification combining radiometrical and the roughness band in test area A: (a) Decorrelation; (b) LS band; (c) 5D band; and (d) MCA-6 band. Red colour represents the background, green colour the motif; and blue colour the geometrical alterations on the rock surface. (For interpretation of the references to color in this figure legend, the reader is referred to the web version of this article.)

Table 6
Percentage of pixels belonging to each informational classes (combining radiometric and roughness bands).

Class	Test area	Decorrelation	LS	5D	MCA-6
Background	A	–	76.93	77.93	76.89
	B	–	79.73	82.49	79.80
	C	–	78.88	79.71	80.08
Motif	A	15.60	15.75	14.74	15.78
	B	10.64	13.49	10.73	13.42
	C	19.28	19.99	19.16	18.79
Geometrical accidents (Roughness band)	A	–	7.33	7.33	7.33
	B	–	6.78	6.78	6.78
	C	–	1.13	1.13	1.13

Table 7
Percentage of pixels belonging to each informational classes (combining radiometric and curvature bands).

Class	Test area	Decorrelation	LS	5D	MCA-6
Background	A	–	81.58	82.50	81.63
	B	–	82.65	85.49	82.67
	C	–	77.87	78.53	79.01
Motif	A	15.60	15.84	14.92	15.79
	B	10.64	13.68	10.84	13.66
	C	19.28	19.97	19.31	18.83
Geometrical accidents (Curvature bands)	A	–	2.58	2.58	2.58
	B	–	3.67	3.67	3.67
	C	–	2.16	2.16	2.16

Table 8
Percentage of pixels belonging to Motif class after considering the geometrical bands (Roughness and Curvature).

Method	Sensor	Geometrical Layer	A (%)	B (%)	C (%)
Decorrelation	Canon 5D	–	15.60	10.64	19.28
Unsupervised classification	Laser Scanner	Roughness	16.45	11.78	19.99
		Curvature	16.49	11.84	19.97
	Canon 5D	Roughness	15.54	10.84	19.16
		Curvature	15.30	10.88	19.31
	Mini MCA – 6	Roughness	16.30	11.77	18.79
		Curvature	16.43	11.83	18.82

were considered as ground truth. This algorithm transforms the initial colour values through the Kafhumen-Loève theorem, reducing the correlation between the RGB channels of the camera and remarking the differences between the radiometric information captured by the spectral bands. Decorrelated the RGB channels, a manual classification of the results, by an expert, was carried out (Fig. 8).

Table 9
Quantitative evaluation of the results obtained during the radiometric classification (initial stage) and its improvement with the geometrical layers (refined stage).

Sensor	Test area	Motif error (%)		
		Initial Stage	Refined Stage Roughness	Refined Stage Curvature
Laser Scanner	A	14.68	5.40	5.83
	B	44.20	12.69	13.23
	C	3.10	1.97	2.10
Canon 5D	A	14.60	0.23	0.73
	B	42.14	0.22	0.25
	C	5.50	5.35	6.06
Mini MCA – 6	A	15.79	5.31	5.61
	B	45.85	13.34	13.14
	C	6.94	7.70	7.87

According with the results obtained (Table 5) (Fig. 8), it is possible to observe that, topographic accidents such as voids are classified in the same class than the motif class, being more evident in the passive bands (5D and MCA-6) (Fig. 8). This comes to reinforce the need to use additional layers able to detect and classify the voids as well as other geometrical accidents.

Geometrically, rock areas affected by the presence of cracks or voids are characterized by local changes of curvature and/or roughness. Considering this assumption, a hybrid classification, combining the radiometry and the geometry of the areas evaluated was carried out. To this end, the geometrical operators defined in Section 2.2, Gaussian curvature and roughness, were used.

According with this new consideration, a total of three informational classes were taken into account: Motif; Background and Geometrical accidents. Previously to the hybrid classification, a sensitivity analysis was performed testing the influence of the kernel size used to generate this geometrical information.

The results of the sensitivity analysis suggest that the best kernel size for the roughness and Gaussian curvature is 0.05 m. Extracted the geometrical information of the test areas, a projection of these values on to the orthoimages was performed, obtaining as a result two additional layers registered in the same coordinate system than the rest of the bands. These additional bands enclose the geometrical information of the motifs and its surroundings (Fig. 9) (Table 6) (Table 7).

Finally and extracted the three thematic classes, a minimum user interaction was required with the aim of classifying all those connected groups presented in the geometrical accidents class to the motif or background classes (Table 8).

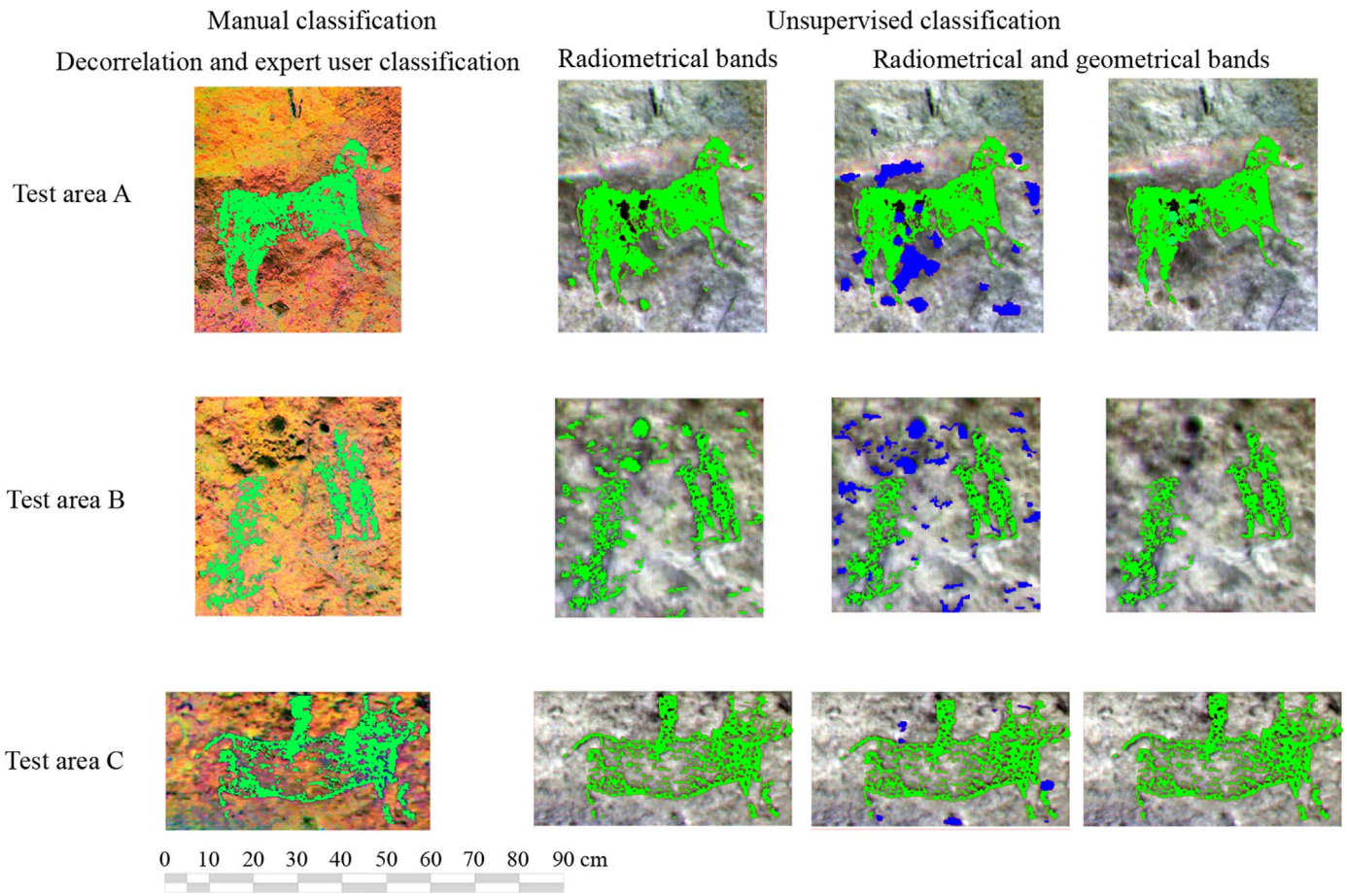

Fig. 10. Qualitative analysis of the results obtained along the different radiometric analysis carried out with Mini MCA-6 multispectral camera (false colour made with bands 10th-5th-7th).

With the aim of evaluating the performance of the results obtained during the different classifications carried out, two quality analysis were used: (i) quantitative analysis to evaluate the number of pixels classified as motif; and (ii) qualitative analysis, observing the similarity between the motif traces extracted with the decorrelation strategy and those extracted with the unsupervised classifications.

On this basis, it is possible to observe an overall improvement of the results obtained during the unsupervised classification adding geometrical layers (Table 9) (Fig. 10). In particular, for test areas A and B, important quantitative and qualitative improvements were observed. For test area C, no improvement was observed on the quantitative results, meanwhile an improvement from the qualitative point of view was obtained. Regarding the geometrical bands used (roughness and curvature), both bands show a similar performance, being slightly better in the roughness case.

3.4. Spatial analysis of the Minateda´s rock-shelter

The identification of painted signs using the different bands that compose the orthoimages is not the only requirement for a complete documentation of the art presented in rock-shelters. Especially in Levantine rock-art where the representation of complex narrative scenes is presented (Walker, 1971).

Geometrical aspects such as the influence of accidents on the rock surface, the diagnosis of the rock shelter (Jordá Cerdá, 2009; Ripoll, 1963), the viewpoint from where the rock-art was conceived or the identification of potential compositions and scenes are aspects to be considered. These aspects can be analyzed through the evaluation of the geometrical features presented in the point cloud at different scales: motif scale and rock-shelter scale.

3.4.1. Analysis of geometric aspects at motif scale

Trying to find a relationship between the detailed rock surface reconstructed and the selection of the areas where the motifs were painted, it could be observed a relationship between the topographic accidents presented and the direction of some of the traces, as well as the morphology of the motifs painted.

Considering the results provided by the pixel-based classification, as well as the geometrical information provided by the digital depth models, we can to relate the traces presented in the motif with the topographic accidents presented in the rock surface. Particularly, the following steps were implemented: (i) traces extraction based on Canny operator (Canny, 1986); (ii) contours lines creation and segmentation with an interval of 5 mm; and (iii) distance evaluation between the motif trace and each contour curve using a threshold of 2 cm. As a result, and after the traces and contour lines extraction, all those edge pixels with a separation higher than 2 cm from the contour line were rejected. Finally, all those groups of connected pixels with less than 50 pixels (about 10 cm) were excluded since they can be considered as non-representative (Fig. 11).

It is possible to observe that part of the horse anatomy (test area A) is influenced by the rock-surface (Fig. 12).

3.4.2. Analysis of geometric aspects at shelter scale

On the other hand, a global analysis of the compositions presented, such as the geometrical disposition of the scene narrated or the relation between the depth of the shelter and the motifs presented on it, are important aspects to understand the rock art presented on the shelter. According with these needs, the following steps were applied: (i) point cloud decimation; (ii) PCA alignment of the point cloud; (iii) depth, roughness and curvature evaluation; (iv) mesh creation; (v) projection

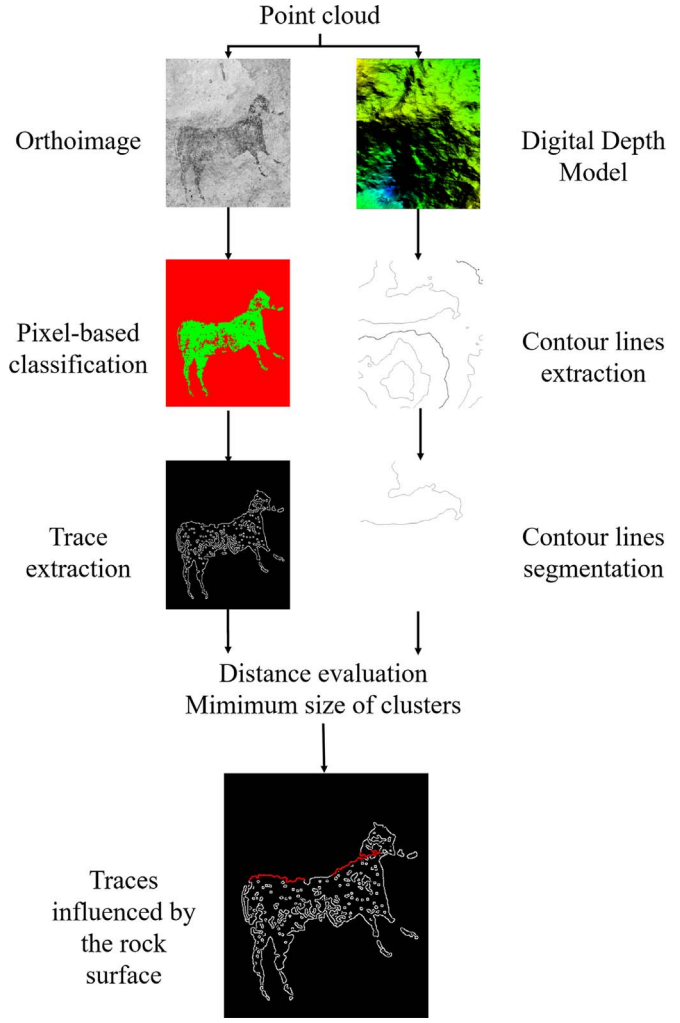

Fig. 11. Schematic representation of the analysis of geometric aspects at motif scale and applied to test area A.

of the results obtained during the radiometric and geometric classification; and (vi) evaluation at global level.

Due to the large amount of data captured (82,244,854 points for the laser scanning and 74,457,717 points for the photogrammetry), a previous decimation of the point cloud was required. To this end a density filter, with a threshold value of 0.01 m, was applied to pass from the raw point cloud to an optimized one, composed by 9,226,243 points in the case of the laser scanning point cloud and 11,286,665 points for the photogrammetric one, representing around the 10% of the original point clouds.

The simplified point clouds obtained by the photogrammetric or laser scanning were referencing in a local coordinate system considering the *X* axis aligned with respect to the longitudinal axis of the rock-shelter, enabling an evaluation between the depth of the shelter and the motifs presented. More precisely, a PCA analysis of the point cloud was carried out, obtaining the direction of maximum dispersion (third Eigen-vector), which corresponds with the longitudinal axis of the shelter. Later, a depth analysis of the shelter was carried out considering a vertical plane along the longitudinal axis of the rock shelter as comparison plane (Fig. 13b).

Since meshes are considered as an ideal product to visualize and consult information derived from geomatic sensors, the simplified and aligned point clouds are converted into meshesusing the Poisson surface reconstruction algorithm (Kazhdan et al., 2006). As a result, a 3D mesh of the rock shelter was obtained with 1,286,637 triangles in the case of the Laser Scanner model and 861,581 triangles for the photogrammetric one. Finally, the information extracted during the radiometric (Fig. 13a) and geometric analysis (Fig. 13b) was mapped over the mesh, allowing the analysis of the possible relationships between the different layers considered: motifs and depth layers.

Due to the large number of motifs presented and since the main focus of the present paper is to highlight the potentialities offered by the proposed method, only a partial mapping of the motifs presented in the shelter was performed. It should be noted that motifs mapped are close to the most protected part of the shelter (Fig. 13b) with an average height of 3.20 m with respect to the rock shelter base. Values higher than the average stature of a Neolithic man (1.65 m) (Ehler and Vancata, 2009). However, the topography presented on the rock-shelter, with a concavity in its central part (Fig. 13b), could be used to paint at this height, since the mean distance between the concavity of the rock shelter and the paintings is 1.20 m. Note also that this area corresponds to a full illuminated area at night, considering a bonfire placed on its central part (Fig. 14a).

As exposed Domingo et al. (2013), one of the main limitations that present traditional two-dimensional techniques for the analysis of rock-art paintings is the difficulty for obtaining different viewpoints and analyses the motifs painted on the shelter, especially in those large and complex caves or shelters. This limitation can be solved with the use of the proposed method, being possible to evaluate the shelter from different viewpoints (Fig. 14b).

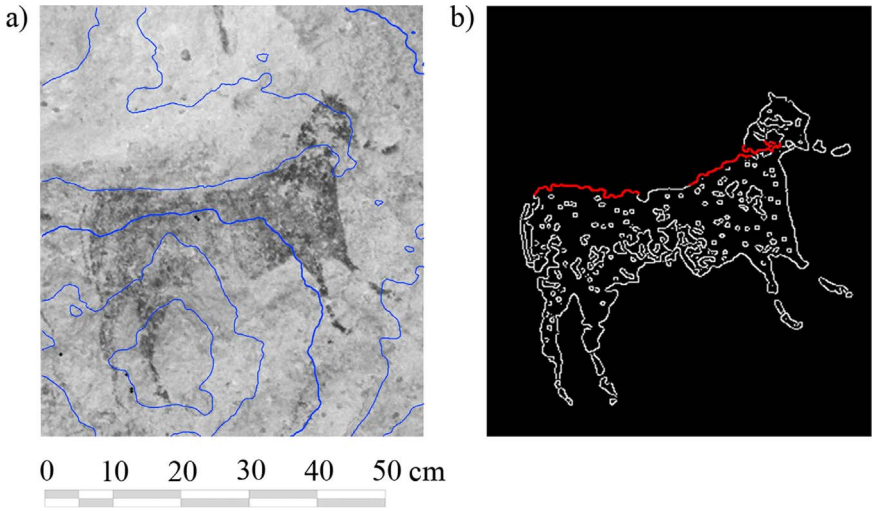

Fig. 12. Results obtained in test area A during the evaluation of the influence of topographic accidents in the horse anatomy.

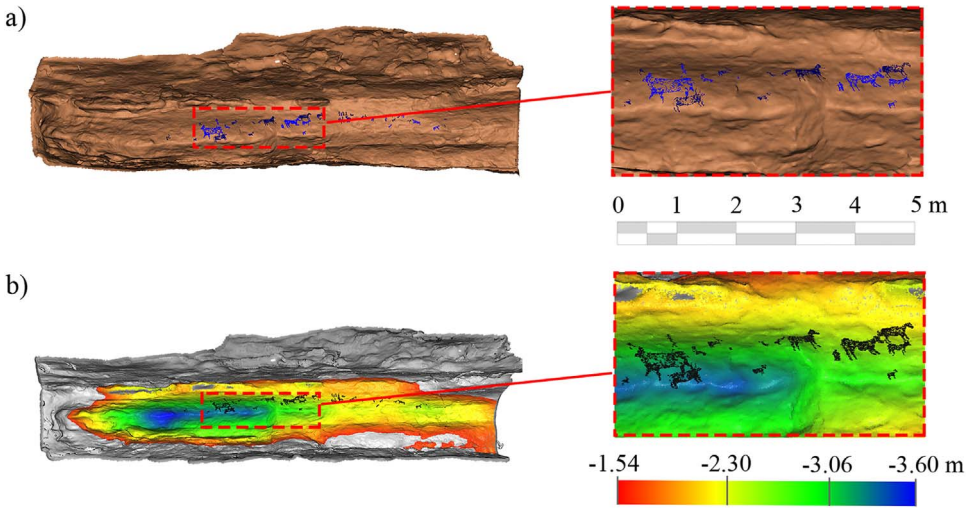

Fig. 13. Mapping of the information obtained during the radiometric and geometric analysis: (a) Partial reconstruction of the motifs presented in the rock-shelter; (b) Visualization of the relationship between the depth and the motifs presented in the rock shelter.

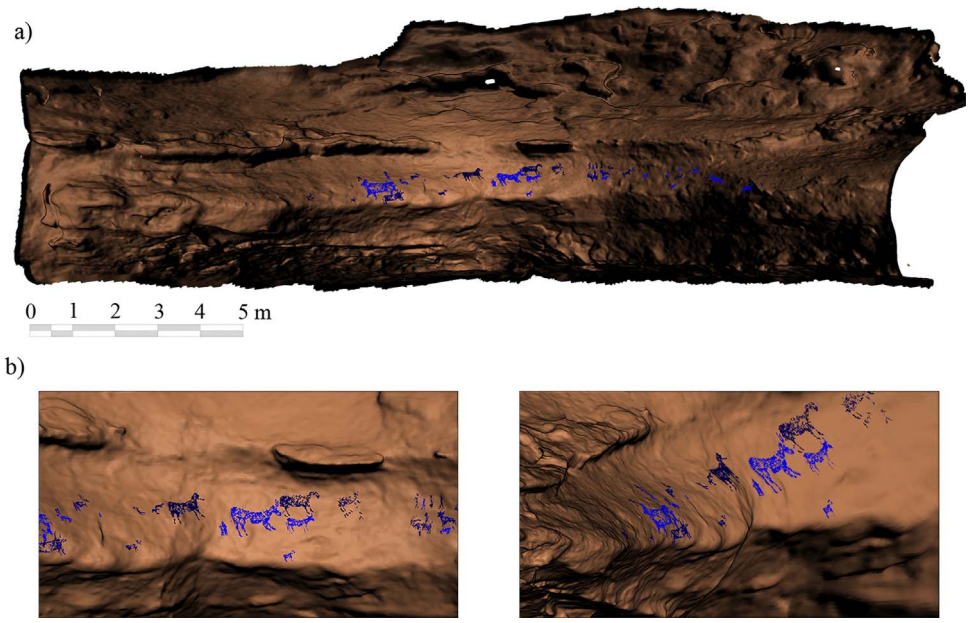

Fig. 14. Different simulations carried out with the model obtained: (a) Simulation of the rock shelter during the night and with a bonfire on the middle; (b) Perspective views from different points during the simulated scene.

4. Conclusions

In this paper a new approach based on the combination of radiometrical and geometrical features for the evaluation of rock art paintings has been presented. The density, accuracy and the radiometric values of the point clouds captured by geomatic sensors such as laser scanner systems, RGB and multispectral cameras can be used to evaluate the motifs presented on a scene at local and global level.

Our approach requires less user interaction in comparison with common practices (Decorrelation Stretch or PCA analysis), being possible to work not only with multispectral data, but also with the geometry of the evaluated areas and allowing the extraction of voids or cracks. Regarding the geometric layers, roughness and Gaussian curvature, both prove to be efficient strategies improving the results obtained during the pixel-based classification: from an average accuracy of 84.98% (test area A), 55.94% (test area B) and 94.82% (test area C) to 96.15%, 91.15% and 94.83%, respectively. With respect to the sensor used, the best results were observed in those classifications that use the Canon 5D bands, probably due to the similarity between the channels used during the Decorrelation Stretch and the pixel-based classification, but also because the analog-to-digital conversion is performed in 14 bits per colour, a substantial increase from the 11 bits of the laser Faro Focus. In addition, the on-chip RGB colour filter uses a standard Bayer pattern over the sensor elements which prevents the false colour and the presence of noise.

Additionally to these geometrical strategies, the present article presents a method able to relate the topographic accidents presented on the rock surface with the quality of the traces is presented, increasing the wide variety of useful information that can be extracted through the proposed method, such as the relation between the rock shelter depth and the location of motifs. All this information can be visualized and consulted easily through the use of a multilayer mesh model.

Inside this wide variety of features (radiometric and geometric) that can be extracted by the proposed method, further investigations could be focused on the dissemination through 3D printed models or the analysis through time by means of 3DGIS tools, as well as the evaluation of other pathological processes such as the presence of

biological organisms.

Acknowledgements

This paper has been developed in the framework of the research project “Infraestructura de datos espaciales de patrimonio arqueológico de Castilla-La Mancha” (POII-2014-004-P) of the 2014–2017 Scientific Research Projects cofounded by the European Regional Development Fund.

The authors would like to thank the Ministry of Education, Culture and Sport of Castilla-La Mancha. Especially to the Directorate-General for Universities, Research and Innovation, the Directorate-General for Cultural and the Museum of Albacete. Authors would also like to thank Lorenzo Abad Casal (University of Alicante), Sonia Gutiérrez Lloret (University of Alicante), Rubí Sanz Gamo (Museum of Albacete) and Blanca Gamo Parras (Museum of Albacete) for their valuable support during the course of this study.

References

Aguilera, D., Lahoz, J., Finat, J., Martinez, J., Fernandez, J., San Josem, J., 2006. Terrestrial laser Canning and low-cost aerial photogrammetry in the archeological modeling of a Jewish tanneries, ISPRS Commission V Symposium Image Engineering and Vision Metrology, Dresden. Citeseer, p. 27.

Azema, M., Gely, B., Bourrillon, R., Lhomme, D., 2013. La grotte ornée paléolithique de Baume Latrone (Gard, France): la 3D remonte le temps…. Palethnologie n°5, 244–246.

Bay, H., Ess, A., Tuytelaars, T., Van Gool, L., 2008. Speeded-up robust features (SURF). Comput. Vision. Image Underst. 110, 346–359.

Besl, P.J., McKay, N.D., 1992. Method for registration of 3-D shapes, Robotics-DL tentative. Int. Soc. Opt. Photonics 586–606.

Bourdier, C., Fuentes, O., Pinçon, G., 2015. Contribution of 3D technologies to the analysis of form in late palaeolithic rock carvings: the case of the Roc-aux-Sorciers rock-shelter (Angles-sur-l’Anglin, France). Digit. Appl. Archaeol. Cult. Herit. 2, 140–154.

Breuil, H., 1920. Les peintures rupestres de la péninsule Ibérique: Les roches peintes de Minateda (Albacete). XI. Masson et Cie.

Burens, A., Grussenmeyer, P., Guillemin, S., Carozza, L., Bourrillon, R., Petrognani, S., 2011. Numérisation 3D de la grotte des Fraux (Saint-Martin-de-Fressengeas, Dordogne, France): approche multiscalaire. In: Jaillet, S., Ployon, E., Villemin, T. (Eds.), Images et modèles 3D en milieux naturels. Edytem, université de Savoie, Chambery, pp. 183–190 (Collection Edytem, no 12).

Canny, J., 1986. A computational approach to edge detection. IEEE Trans. Pattern Anal. Mach. Intell. 679–698.

Cefalu, A., Abdel-Wahab, M., Peter, M., Wenzel, K., Fritsch, D., 2013. Image based 3D reconstruction in Cultural heritage preservation. ICINCO 1, 201–205.

Cerrillo-Cuenca, E., Sepúlveda, M., 2015. An assessment of methods for the digital enhancement of rock paintings: the rock art from the precordillera of Arica (Chile) as a case study. J. Archaeol. Sci. 55, 197–208.

Defrasne, C., 2014. Digital image enhancement for recording rupestrian engravings: applications to an alpine rockshelter. J. Archaeol. Sci. 50, 31–38.

Del Pozo-Aguilera, S., Herrero-Pascual, J., Felipe-García, B., Hernández-López, D., Rodríguez-Gonzálvez, P., González-Aguilera, D., 2016. Multispectral Radiometric Analysis of Façades to Detect Pathologies from Active and Passive Remote Sensing. Remote Sens. 8, 80.

Domingo, I., Villaverde, V., López-Montalvo, E., Lerma, J.L., Cabrelles, M., 2013. Latest developments in rock art recording: towards an integral documentation of Levantine rock art sites combining 2D and 3D recording techniques. J. Archaeol. Sci. 40, 1879–1889.

Domingo, I., Carrión, B., Blanco, S., Lerma, J.L., 2015. Evaluating conventional and advanced visible image enhancement solutions to produce digital tracings at el Carche rock art shelter. Digit. Appl. Archaeol. Cult. Herit. 2, 79–88.

Ehler, E., Vancata, V., 2009. Neolithic transition in Europe: evolutionary anthropology study. Anthropologie 47, 185.

Fernández-Hernandez, J., González-Aguilera, D., Rodríguez-Gonzálvez, P., Mancera-Taboada, J., 2015. Image-Based Modelling from Unmanned Aerial Vehicle (UAV) Photogrammetry: an Effective, Low-Cost Tool for Archaeological Applications. Archaeometry 57, 128–145.

Fritz, C., Willis, M.D., Tosello, G., 2016. Reconstructing Paleolithic cave art: the example of Marsoulas cave (France). J. Archaeol. Sci.: Rep.

Gomez-Lahoz, J., Gonzalez-Aguilera, D., 2009. Recovering traditions in the digital era: the use of blimps for modelling the archaeological cultural heritage. J. Archaeol. Sci. 36, 100–109.

González-Aguilera, D., López-Fernández, L., Rodriguez-Gonzalvez, P., Guerrero, D., Hernandez-Lopez, D., Remondino, F., Menna, F., Nocerino, E., Toschi, I., Ballabeni, A., Gaiani, M., 2016. DEVELOPMENT OF AN all-purpose free PHOTOGRAMMETRIC tool. Int. Arch. Photogramm. Remote Sens. Spat. Inf. Sci. XLI-B6, 31–38.

Herbert, D.T., 1995. Heritage, tourism and society. Mansell Publishing.

Jordá Cerdá, F., 2009. Formas de vida económica en el arte rupestre levantino.

Kazhdan, M., Bolitho, M., Hoppe, H., 2006. Poisson surface reconstruction, In: Proceedings of the fourth Eurographics symposium on Geometry processing.

Kraus, K., 2007. Photogrammetry: geometry from images and laser scans. Walter de Gruyter.

Le Quellec, J.-L., Duquesnoy, F., Defrasne, C., 2015. Digital image enhancement with DStretch: is complexity always necessary for efficiency? Digit. Appl. Archaeol. Cult. Herit.

Lejeune, M., 1985. La paroi des grottes, premier "mur" support artistique et document archéologique. Le mur dans l’art et l’archéologie. Art. Et. Fact., n°2. Liège 15–24.

Lerma, J.L., Navarro, S., Cabrelles, M., Seguí, A.E., Hernández, D., 2013. Automatic orientation and 3D modelling from markerless rock art imagery. ISPRS J. Photogramm. Remote Sens. 76, 64–75.

López-Montalvo, E., Sanz, I.D., 2005. Nuevas tecnologías y restitución bidimensional de los paneles levantinos: primeros resultados y valoración crítica del método, Actas del III Congreso del Neolítico en la Península Ibérica: Santander, 5 a 8 de octubre de 2003. Serv. De. Publ. 719–728.

Lowe, D.G., 1999. Object recognition from local scale-invariant features, Computer vision, 1999. In: Proceedings of the seventh IEEE international conference on. Ieee, pp. 1150–1157.

Magid, E., Soldea, O., Rivlin, E., 2007. A comparison of Gaussian and mean curvature estimation methods on triangular meshes of range image data. Comput. Vision. Image Underst. 107, 139–159.

Mas, M., Jorge, A., Gavilán, B., Solís, M., Parra, E., Pérez, P.-P., 2013. Minateda rock shelters (Albacete) and post-palaeolithic art of the Mediterranean Basin in Spain: pigments, surfaces and patinas. J. Archaeol. Sci. 40, 4635–4647.

Montés, J.F.J., 2010. El caballo en el arte rupestre levantino de la península ibérica. El santuario rupestre de Minateda y sus probables arquetipos iconográficos del paleolítico superior. Quaderns de prehistòria i arqueologia de Castelló 28, 7–38.

Pierrot-Deseilligny, M., Rupnik, E., Girod, L., Belvaux, J., Maillet, G., Deveau, M., Choqueux, G., 2015. MicMac, Apero, Pastis and Other Beverages in a Nutshell. ENSG, IGN, Champs-Sur-Marne, France.

Pinçon G., Bourdier C., Fuentes O., Abgrall A., 2010. De la manipulation des images 3D. In: In Situ [En ligne], 13.

Puchol, O.G., McClure, S.B., Senabre, J.B., Villa, F.C., Porcelli, V., 2013. Increasing contextual information by merging existing archaeological data with state of the art laser scanning in the prehistoric funerary deposit of Pastora Cave, Eastern Spain. J. Archaeol. Sci. 40, 1593–1601.

Ripoll, E., 1963. Pinturas rupestres de la Gasulla (Castellón). Monografías de Arte Rupestre. Arte Levantino 2.

Robert E., 2016. Le rôle du support dans la construction des images au sein l’art paléolithique européen, in Groenen (M., dir.), Styles, techniques and graphic expression in rock art, Actes de la session du 17ème congrès mondial de l’UISPP, British Archaeological Reports, pp. 174–195.

Robert, E., Petrognani, S., Lesvignes, E., 2016. Applications of digital photography in the study of Paleolithic cave art. J. Archaeol. Sci.: Rep.

Rodríguez-González, P., Garcia-Gago, J., Gomez-Lahoz, J., González-Aguilera, D., 2014. Confronting passive and active. Sens. Non-Gaussian Stat. Sens. 14, 13759.

Rodríguez-González, P., Nocerino, E., Menna, F., Minto, S., Remondino, F., 2015. 3D SURVEYING & modeling OF underground passages IN WWI FORTIFICATIONS. Int. Arch. Photogramm. Remote Sens 17–24.

Rodríguez-González, P., Mancera-Taboada, J., González-Aguilera, D., Muñoz-Nieto, Á., Armesto, J., 2012. A hybrid approach to create an archaeological visualization system for a Palaeolithic cave. Archaeometry 54, 565–580.

Rodríguez-Martín, M., Rodríguez-González, P., Lagüela, S., González-Aguilera, D., 2016. Macro-photogrammetry as a tool for the accurate measurement of three-dimensional misalignment in welding. Autom. Constr. 71, 189–197.

Rogerio-Candelera, M.Á., 2015. Digital image analysis based study, recording, and protection of painted rock art. Some Iberian experiences. Digit. Appl. Archaeol. Cult. Herit. 2, 68–78.

Sánchez-Aparicio, L.J., Riveiro, B., Gonzalez-Aguilera, D., Ramos, L.F., 2014. The combination of geomatic approaches and operational modal analysis to improve calibration of finite element models: a case of study in Saint Torcato Church (Guimarães, Portugal). Constr. Build. Mater. 70, 118–129.

Sauvet G., Tosello G., 1998. Le mythe paléolithique de la caverne, in Sacco F., Sauvet G. dir., Le propre de l’homme, Psychanalyse et préhistoire, Paris, Delachaux et Niestlé, coll. Champs psychanalytiques, pp. 55–90.

Seidl, M., Wieser, E., Alexander, C., 2015. Automated classification of petroglyphs. Digit. Appl. Archaeol. Cult. Herit. 2, 196–212.

Toldo, R., Beinat, A., Crosilla, F., 2010. Global registration of multiple point clouds embedding the Generalized Procrustes Analysis into an ICP framework, 3DPVT 2010 Conference.

Tombari, F., Di Stefano, L., 2014. Interest Points via Maximal Self-Dissimilarities, Asian Conference on Computer Vision. Springer, pp. 586–600.

Torres-Martínez, J.A., Seddaiu, M., Rodríguez-González, P., Hernández-López, D., González-Aguilera, D., 2016. A multi-data source and multi-sensor approach for the 3D reconstruction and web visualization of a complex Archaelogical site: the case study of “Tolmo De Minateda”. Remote Sens. 8, 550.

Walker, M., 1971. Spanish levantine rock art. Man 553–589.

Zeppelzauer, M., Poier, G., Seidl, M., Reinbacher, C., Breiteneder, C., Bischof, H., Schulter, S., 2015. Interactive segmentation of rock-art in high-resolution 3D reconstructions, 2015 digital heritage. IEEE 37–44.